Stem-Loop Structures within mRNA Coding Sequences Activate Translation Initiation and Mediate Control by Small Regulatory RNAs

Jonathan Jagodnik, Claude Chiaruttini, Maude Guillier

Article

Molecular Cell

Stem-Loop Structures within mRNA Coding Sequences Activate Translation Initiation and Mediate Control by Small Regulatory RNAs

Graphical Abstract

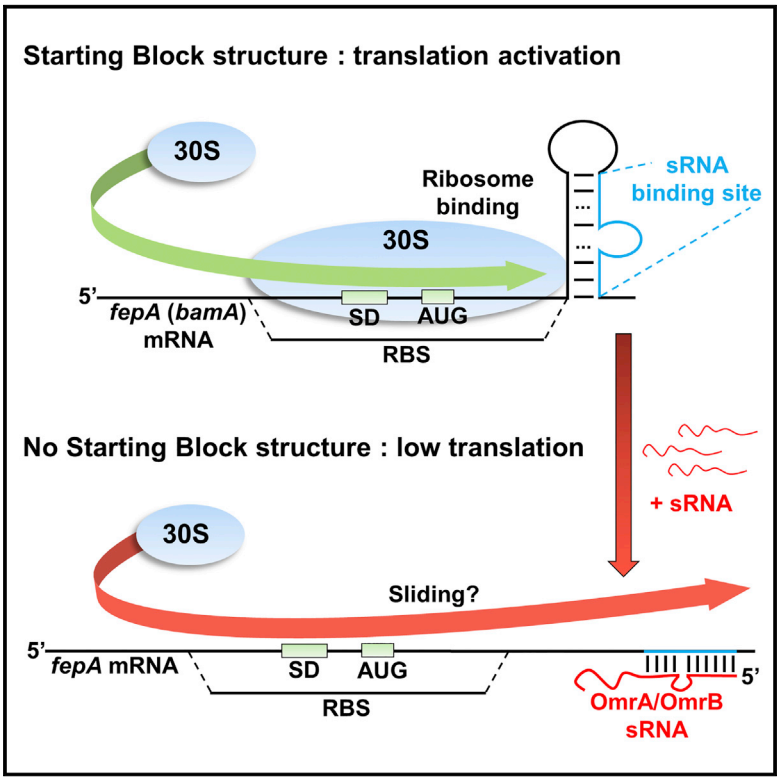

Highlights

- A stem-loop within *E. coli fepA* mRNA coding region activates translation initiation
- A similar activating stem-loop structure exists within *bamA* mRNA coding region
- These stem-loops activate translation independently of their nucleotide sequence
- Small RNAs repress *fepA* expression by targeting its activating structure

Authors

Jonathan Jagodnik, Claude Chiaruttini, Maude Guillier

Correspondence

maude.guillier@ibpc.fr

In Brief

Jagodnik et al. report here that stem-loop structures located within the early ORF of bacterial mRNAs can activate translation initiation, independently of their nucleotide sequence. This strikingly contrasts with the established inhibition of translation by secondary structures. Furthermore, small RNAs can target these activating structures to control gene expression.

Jagodnik et al., 2017, Molecular Cell *68*, 1–13
October 5, 2017
http://dx.doi.org/10.1016/j.molcel.2017.08.015

CellPress

Please cite this article in press as: Jagodnik et al., Stem-Loop Structures within mRNA Coding Sequences Activate Translation Initiation and Mediate Control by Small Regulatory RNAs, Molecular Cell (2017), http://dx.doi.org/10.1016/j.molcel.2017.08.015

Molecular Cell
Article

Stem-Loop Structures within mRNA Coding Sequences Activate Translation Initiation and Mediate Control by Small Regulatory RNAs

Jonathan Jagodnik,[1] Claude Chiaruttini,[1] and Maude Guillier[1,2,*]
[1]CNRS UMR8261, Associated with University Paris Diderot, Sorbonne Paris Cité, Institut de Biologie Physico-Chimique, 75005 Paris, France
[2]Lead Contact
*Correspondence: maude.guillier@ibpc.fr
http://dx.doi.org/10.1016/j.molcel.2017.08.015

SUMMARY

Initiation is the rate-limiting step of translation, and in bacteria, mRNA secondary structure has been extensively reported as limiting the efficiency of translation by occluding the ribosome-binding site. In striking contrast with this inhibitory effect, we report here that stem-loop structures located within coding sequences instead activate translation initiation of the *Escherichia coli fepA* and *bamA* mRNAs involved in iron acquisition and outer membrane proteins assembly, respectively. Both structures promote ribosome binding *in vitro*, independently of their nucleotide sequence. Moreover, two small regulatory RNAs, OmrA and OmrB, base pair to and most likely disrupt the *fepA* stem-loop structure, thereby repressing FepA synthesis. By expanding our understanding of how mRNA *cis*-acting elements regulate translation, these data challenge the widespread view of mRNA secondary structures as translation inhibitors and show that translation-activating elements embedded in coding sequences can be targeted by small RNAs to inhibit gene expression.

INTRODUCTION

Successful adaptation of bacteria to multiple niches relies on their ability to rapidly and precisely tune gene expression in response to extremely diverse environmental cues. While control can occur at virtually all stages of the gene expression pathway, regulating translation and/or the stability of target mRNAs offers several advantages for adaptive responses, in particular, the speed of response by acting directly at the mRNA level, and the possibility to prevent transcriptional noise or to differentially regulate individual cistrons within an operon.

An important feature of post-transcriptional control is the wide diversity of underlying molecular mechanisms and regulators, in line with the remarkable plasticity of mRNAs, which are the controlled targets. This is particularly well illustrated by the plethora of small regulatory RNAs (sRNAs) identified in bacteria, many of which base pair via short and imperfect duplexes to target mRNAs and thereby modulate their translation and/or stability (Wagner and Romby, 2015). In enterobacteria, these imperfectly pairing sRNAs most often require an RNA chaperone called Hfq that stabilizes many sRNAs and facilitates sRNA-mRNA duplex formation (Vogel and Luisi, 2011). Interestingly, sRNAs have been shown to negatively or positively control gene expression using a remarkable variety of molecular mechanisms (Jagodnik et al., 2017).

In the most frequent scenario, sRNAs repress the expression of targets by binding at or in the vicinity of the ribosome-binding site (RBS), thereby directly competing with the 30S ribosomal subunit for binding to the mRNA. However, they can also affect the accessibility of the RBS when they base pair outside of this region by inducing structural changes that ultimately lead to a more or less accessible Shine-Dalgarno (SD) region and thus to a positive (Mandin and Gottesman, 2010 and references therein) or negative (Heidrich et al., 2007) control. Furthermore, the primary effect of sRNA binding to mRNAs is not necessarily translational: sRNAs have been reported to mediate target mRNA destabilization by guiding the endoribonuclease RNase E to the mRNA, for instance (Bandyra et al., 2012; Pfeiffer et al., 2009), or, in contrast, to stabilize target mRNAs (Obana et al., 2010; Papenfort et al., 2013; Ramirez-Peña et al., 2010). Yet, other mechanisms have been described that bring new insight into translation mechanisms. For instance, the study of IstR sRNA repression of *tisB* mRNA expression identified a ribosome stand-by site that allows translation from a downstream translation initiation region (TIR) that is sequestered in a stem-loop structure (Darfeuille et al., 2007). A variation on this theme was later proposed for the translational activation of *iroN* by the *Salmonella* RyhB sRNA homologs that would allow entry of the ribosome at an upstream stand-by site (Balbontín et al., 2016).

OmrA and OmrB are two Hfq-dependent sRNAs conserved in enterobacteria. Their transcription is activated by the OmpR regulator, either in its phosphorylated form or under high concentrations of its non-phosphorylated form (Brosse et al., 2016). The transcription of *omrA* has also been shown to specifically respond to the RpoS sigma factor (Lévi-Meyrueis et al., 2014; Peano et al., 2015). OmrA and OmrB target several mRNAs by base pairing interaction via their almost identical 5′ ends, which are highly conserved in other bacteria. As a consequence, all the target mRNAs described so far, all negatively regulated, are common to both sRNAs. Several of these targets encode transcriptional regulators, such as CsgD and FlhDC, the master

regulators of curli and flagella synthesis, respectively, or the EnvZ-OmpR two-component system (TCS), i.e., the Omr transcriptional activator (Brosse et al., 2016; De Lay and Gottesman, 2012; Holmqvist et al., 2010). In addition, OmrA/B downregulate the synthesis of several outer membrane proteins (OMPs): OmpT, CirA, FecA, and FepA (Guillier and Gottesman, 2006, 2008). While OmpT is a protease, CirA, FecA, and FepA are receptors for iron-siderophore complexes involved in iron uptake. In line with this function, *cirA*, *fecA*, and *fepA* genes are members of the Fur regulon, and their transcription is induced under conditions of iron deprivation. In addition, synthesis of CirA also responds to iron starvation at the post-transcriptional level—this time positively—through translational activation mediated by the Fur-repressed RyhB sRNA (Salvail et al., 2013). These three receptors bind to different siderophores, and FepA is likely to play a key role in iron homeostasis, as it is the receptor for iron chelated by enterobactin, i.e., the most potent siderophore.

From a mechanistic standpoint, the Omr sRNAs were shown to pair with the TIR of *ompT*, *cirA*, *ompR-envZ*, and *flhDC* mRNAs, thus presumably repressing their translation by the classical mechanism of competition with ribosome binding. However, the question of how the Omr achieved regulation of *fecA* and *fepA* genes has not yet been addressed. This question appears all the more pertinent as (1) OmrA/B were previously shown to repress *csgD* expression by targeting the *csgD* mRNA outside of the TIR (Holmqvist et al., 2010) and (2) there is no obvious complementarity between the Omr 5′ ends and the TIR of *fecA* or *fepA* mRNA.

In the present work, we have investigated the mechanism of *fepA* control by OmrA/B in detail and found that both sRNAs target a stem-loop (SL) structure within the *fepA* mRNA coding sequence. Unexpectedly, this SL activates translation initiation by promoting formation of the pre-initiation complex between the *fepA* mRNA, the 30S ribosomal subunit, and the initiator tRNA. Introduction of compensatory changes within the SL further indicated that this effect is independent of its nucleotide sequence. Importantly, similar SL can be predicted in several bacterial mRNAs, and we have shown that the one in the essential *bamA* gene also activates translation initiation. By uncovering the positive role played by secondary structures of the mRNA, these results shed a new light on the translation initiation step in bacteria and the role of mRNA *cis*-elements in this process.

RESULTS

OmrA/B Directly Repress *fepA* Expression by Base Pairing within Its Coding Sequence

We previously showed that pulse-induction of OmrA/B led to a decrease in *fepA* mRNA levels, suggesting that *fepA* might be a direct target of these sRNAs (Guillier and Gottesman, 2006, 2008). This prompted us to search for possible base pairing between *fepA* and OmrA/B using IntaRNA (Wright et al., 2014) and TargetRNA (Kery et al., 2014) programs. Because a mutant in the 5′ end of OmrA/B no longer affected *fepA* mRNA levels (Guillier and Gottesman, 2008), we only used the 20 conserved 5′ end nucleotides of OmrA/B for this search; the *fepA* mRNA fragment used encompassed nucleotides −173 (which corresponds to the transcription start site) to +80 (+1 being the first nucleotide of *fepA* open reading frame [ORF]). The resulting prediction, with some manual adjustment, shows that nucleotides 1 to 26 of OmrA/B can potentially pair imperfectly with nucleotides 23 to 44 of *fepA* ORF (Figure 1A). The existence of this interaction was further validated using a translational *fepA-lacZ* fusion, where *fepA* 5′ UTR and first 45 nt of the ORF were fused upstream of the 10th codon of *lacZ*. This protein fusion is constitutively expressed from a P_{tet} promoter (Figure 1B). Overproduction of OmrA or OmrB reduced expression of this fusion by 8.3- and 4.7-fold, respectively (Figure 1C). This reduction was no longer observed when mutations were introduced in the regions predicted to pair, either in nucleotides 3–6 of OmrA/B or in nucleotides 39–42 of the *fepA* ORF. Importantly, these mutant forms of the Omr sRNAs accumulate to even higher levels than their wild-type (WT) counterparts, and the loss in repression is thus not due to differential levels of the different sRNAs (Figure S1A). A combination of these mutations, which re-establishes base pairing, partially restored control: OmrA/Bmut repressed *fepAmut-lacZ* by 2.7- and 1.8-fold, respectively (Figure 1C). These data strongly support the *in vivo* interaction between OmrA/B 5′ ends and the proximal region of the *fepA* ORF. This regulation was confirmed by directly following the levels of the FepA protein made from its endogenous locus during a short overexpression of OmrA/B sRNA. More precisely, cells transformed with OmrA/B-overexpressing plasmid were grown to mid-exponential phase and split in two, and half of the culture was treated with 250 μM 2-2′-dipyridyl (dip) and 100 μM isopropyl β-D-thiogalactopyranoside (IPTG) to induce *fepA* expression and OmrA/B synthesis, respectively. As a control, the other half of the culture was left untreated. After 15 min, proteins and RNA samples were extracted, and the levels of FepA protein and of OmrA and OmrB sRNAs were followed by western or northern blot analysis, respectively. In the presence of the vector control, addition of dip induced FepA synthesis, as expected since *fepA* transcription is Fur repressed. This induction was strongly reduced in presence of plasmids overexpressing either WT OmrA or OmrB but was completely restored when the mutant versions of OmrA/B, which accumulate at similar levels compared to their WT counterparts, were overexpressed instead (Figure 1D). OmrA/B sRNAs thus specifically and rapidly repress synthesis of the FepA protein via base-pairing interaction.

Only Short Regions of *fepA* mRNA and of OmrA/B Are Involved in the Interaction

Identification of one site of interaction between a sRNA and its target mRNA does not rule out the existence of other secondary pairing sites. We therefore asked whether other regions of *fepA* or of the Omr sRNAs were required for control. We first analyzed the repression of a shorter *fepA-lacZ* fusion lacking most of the *fepA* 5′ UTR (*fepA*$_{-26}$ in Figure 1B). Expression of this fusion was repressed by OmrA/B as efficiently as the longer fusion (Figure 1E), showing that most of the *fepA* 5′ UTR is dispensable for control. To then determine whether the 5′ end of OmrA/B is the only region involved in pairing with *fepA* mRNA, we used a chimeric sRNA construct called OmrY, which consists of the first 15 nt of OmrA/B followed by the last 61 nt of the RybB sRNA (Figure 1F). As RybB is an Hfq-dependent sRNA that regulates most

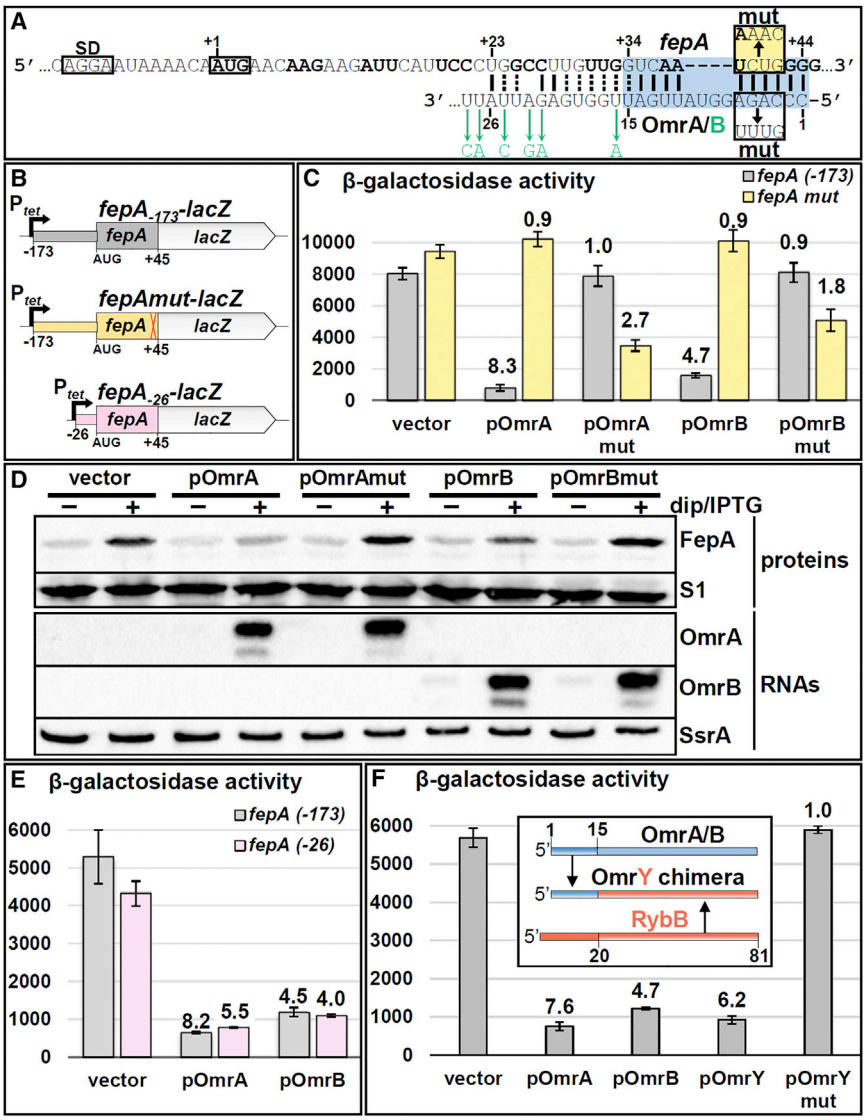

Figure 1. Direct Repression of *fepA* Expression by the 5′ End of OmrA/B Relies on a Short Interaction within *fepA* ORF

(A) Predicted base pairing between *fepA* mRNA and OmrA/B sRNAs. Successive black and gray codons indicate *fepA* reading frame. OmrB nucleotides that differ from OmrA are shown below the OmrA sequence. The mutations introduced in *fepA-lacZ* or in OmrA/B are boxed (mut). The pairing region shown to be necessary and sufficient for regulation is highlighted in blue.

(B) Various *fepA-lacZ* translational fusions used in this study. Positions on *fepA* mRNA are given relative to the start codon.

(C) β-galactosidase activities of *omrAB* deleted strains carrying the $fepA_{-173}$-*lacZ* (strain JJ0015) or *fepAmut-lacZ* (strain JJ0019) fusion and transformed with OmrA-, OmrAmut-, OmrB-, or OmrBmut-overexpressing plasmids or a vector control.

(D) Western blot analysis of the FepA protein levels (in strain MG1099) in response to WT or mutant OmrA or OmrB induction. Levels of the different sRNAs were followed by northern blot in the same experiment. *E. coli* ribosomal protein S1 or SsrA RNA were used as loading controls for proteins and RNAs, respectively.

(E) β-galactosidase activities of the $fepA_{-173}$-*lacZ* (strain MG1772) and the $fepA_{-26}$-*lacZ* (strain JJ0135) fusion strains transformed with OmrA- or OmrB-overexpressing plasmids or a vector control.

(F) β-galactosidase activity of the $fepA_{-173}$-*lacZ* (strain JJ0015) fusion strain transformed with OmrA-, OmrB-, OmrY-, or OmrYmut-overexpressing plasmids or a vector control. The framed schematic displays the design of the OmrY chimera: conserved nucleotides 1 to 15 of OmrA/B are fused to nucleotides 20 to 81 of RybB. β-galactosidase activities are expressed in Miller units. Numbers above the bars give the repression factors.

Throughout the manuscript, error bars represent 95% confidence intervals (see STAR Methods for more details).

of its targets via its 5′ end, the resulting OmrY is expected to display the target specificity of OmrA/B while retaining all other properties of an Hfq-dependent sRNA. Overexpression of WT OmrY efficiently repressed expression of the *fepA-lacZ* fusion (Figure 1F), as well as synthesis of the FepA protein (Figure S1B), similar to what is observed with OmrA/B. Furthermore, repression was abolished when nucleotides 3–6 of OmrY were mutated (this did not reduce sRNA levels; Figure S1B), showing that repression by OmrY also primarily relies on its 5′ end and not on regions of the RybB sRNA (Figure 1F). Together, these data suggest that the pairing site between nucleotides 1–15 of OmrA/B and nucleotides 34–44 of *fepA* mRNA is the primary site of interaction and is sufficient to provide full control. Interestingly, the region of *fepA* mRNA targeted by OmrA/B is located within the *fepA* ORF but outside of the region bound by the 30S ribosomal subunit during translation initiation (Hüttenhofer and Noller, 1994; Yusupova et al., 2001), raising the question of the underlying molecular mechanism of control.

RNase E Endonuclease Is Not Required for *fepA* Repression by OmrA/B

Other examples of bacterial sRNAs pairing to coding regions outside of the RBS have been reported previously (Heidrich et al., 2007; Papenfort et al., 2013; Pfeiffer et al., 2009). In the case of the repressive MicC-*ompD* mRNA interaction in *Salmonella*, it was shown that this pairing far from the RBS did not affect translation initiation but instead induced an RNase E-dependent destabilization of the target mRNA (Bandyra et al., 2012; Pfeiffer et al., 2009). This prompted us to investigate whether RNase E was also required for OmrA/B control of *fepA* expression by following the synthesis of FepA protein in WT or rne^{ts} strains transformed with OmrA/B-overexpressing plasmids. In this experiment, cells were grown at 37°C up to mid-exponential phase, and cultures were split in two. One aliquot continued to grow at 37°C as a control; the second was shifted to 44°C for 15 min to inactivate the thermosensitive RNase E, in the presence of 250 μM dip to induce FepA

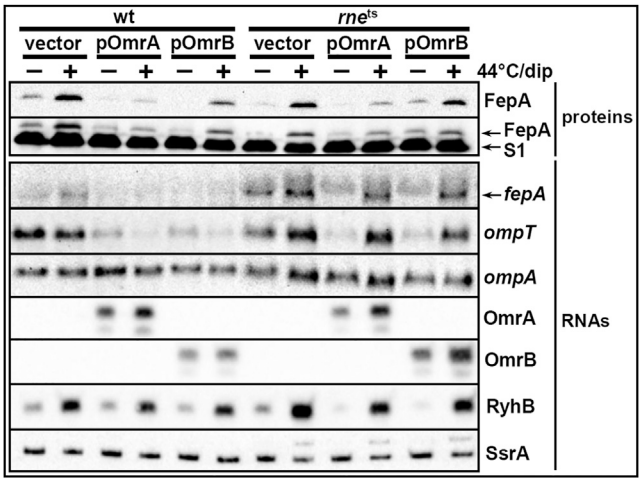

Figure 2. The Regulation of FepA Synthesis by OmrA/B Is RNase E Independent

The levels of FepA protein and of *fepA* mRNA were analyzed in WT or *rne*^{ts} strains overproducing OmrA or OmrB. Strains MG1325 (WT) or MG1326 (*rne*^{ts}) transformed with indicated plasmids were grown at 37°C to mid-exponential phase and either kept at 37°C (−) or shifted to 44°C in the presence of dip (+). Specific proteins and RNAs were then analyzed by western or northern blotting, respectively. Detection of S1 was performed as a loading control after detection of FepA, which explains the presence of the FepA signal. Probing of *ompA* and SsrA RNAs were also loading controls, while monitoring the levels of RyhB sRNA was used as a control for dip induction.

synthesis. Proteins and RNAs were extracted from both aliquots, and specific proteins or mRNAs were analyzed by western or northern blotting, respectively (Figure 2). In WT cells, addition of dip induced FepA synthesis in presence of the empty vector, and induction was reduced upon OmrA/B overproduction, as expected. Strikingly, a highly similar pattern for FepA protein was observed with the empty vector or the OmrA-overproducing plasmid in *rne*^{ts} cells. Inactivation of RNase E activity was confirmed by the fact that *ompT* mRNA was not degraded in response to OmrA/B induction, as previously observed (Guillier and Gottesman, 2008). Thus, RNase E is not required for the control of FepA protein levels by OmrA. For OmrB, control of FepA levels in the *rne*^{ts} mutant was not as efficient as in the *rne*$^{+}$ cells but was nonetheless still visible, suggesting that repression still occurs. While these data are not sufficient to rule out a role for the RNase E in achieving the full range of regulation, especially for OmrB, they nevertheless show that OmrA/B still control the levels of FepA protein in the absence of RNase E. In contrast, the decrease in *fepA* mRNA levels observed upon OmrA/B overproduction clearly required a functional RNase E, suggesting that *fepA* mRNA degradation by RNase E is a consequence of the inhibition of *fepA* translation by OmrA/B.

OmrA/B 5′ End Controls *fepA* Translation Initiation by Inhibition of Ribosome Binding

Even though the previous result did not rule out a primary effect of OmrA/B on *fepA* mRNA stability via the involvement of ribonucleases other than RNase E, it nonetheless led us to investigate whether OmrA/B affected ribosome binding to the *fepA* mRNA. For this purpose, toeprinting experiments were performed on the *fepA*$_{-173}$ transcript extending from nucleotides −173 to +129 to follow the formation of ternary translation initiation complexes *in vitro*, with and without sRNA. Addition of the 30S ribosomal subunit and initiator tRNA induced reverse transcription (RT) stops at positions +15/+16 of the *fepA* ORF (“toeprint” signal in Figure 3A). Despite the fact that only the WT OmrA or OmrB, and not the mutant derivatives, seemed to bind to *fepA* mRNA in this experiment, the toeprint signal was non-specifically decreased in presence of any of these sRNAs (Figure 3A; Figure S2). To circumvent this lack of specificity, the experiment was repeated with OmrA and OmrAmut in the presence of increasing concentrations of the Hfq RNA chaperone. Addition of Hfq alone led to a strong inhibition of the toeprint at high concentrations (Figure 3B). This is again most likely non-specific, as it is not observed in the presence of sRNAs known to strongly bind Hfq, such as OmrA or OmrAmut. Furthermore, when added in conjunction with sRNAs, Hfq both increased formation of the OmrA-*fepA* duplex, as previously observed for other sRNA-mRNA pairs *in vitro* (e.g., Kawamoto et al., 2006), and allowed a specific inhibition of toeprint formation by OmrA (Figure 3B). At this stage, it was not clear whether this was simply due to the stronger binding of OmrA to *fepA* mRNA in the presence of Hfq or whether Hfq could play a more direct role in the translation inhibition.

To discriminate between these possibilities, the experiment was then performed without Hfq and in presence of increasing concentrations of the chimeric OmrY sRNA or the 5′ end mutant variant. OmrY, but not OmrYmut, produced a specific inhibition of the toeprint, possibly due to a stronger binding of OmrY than OmrA/B to the *fepA* mRNA, as it induced a stronger RT stop at nucleotide G+44 of *fepA* ORF (Figure 3A; Figures S2A and S2B). Finally, we also analyzed the effect of a 16-mer DNA oligonucleotide mimicking the 5′ end of OmrA/B, again in the absence of Hfq. This antisense DNA (AsDNA), referred to as As28.43, is perfectly complementary to nucleotides 28 to 43 of the *fepA* ORF, i.e., the nucleotides that base pair with nucleotides 2–6 and 11–21 of OmrA/B (Figure 3C). As28.43 DNA efficiently bound to the *fepA* mRNA *in vitro*, as shown by the RT stop it induced at position G+43, and it strongly inhibited the toeprint, even at the lowest AsDNA/mRNA ratio used in this experiment. And as expected, neither binding nor toeprint inhibition was observed with the mutant derivative of As28.43, showing that the effect of As28.43 is specific (Figure 3D).

Together, these data show that, at least in presence of Hfq, OmrA/B repress *fepA* expression at the level of translation initiation by preventing binding of the 30S ribosomal subunit. Furthermore, the results obtained with OmrY or the short AsDNA indicate that the role of Hfq is limited to facilitating and/or stabilizing duplex formation and that the OmrA/B sequence downstream of nucleotide +15 is dispensable for this effect. In other words, the 5′ end of OmrA/B is sufficient to inhibit translation initiation *in vitro* by pairing within *fepA* ORF downstream of nucleotide +28. Intriguingly, this lies outside of the region bound by the 30S ribosomal subunit during initiation complex formation.

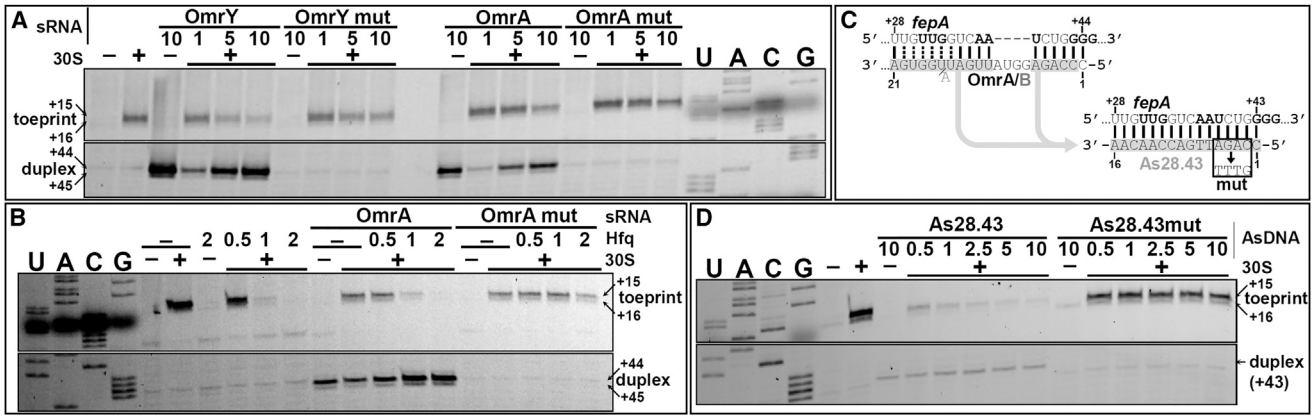

Figure 3. OmrA/B 5′ End Inhibits Binding of the 30S Ribosomal Subunit to *fepA* mRNA

(A and B) Toeprinting assays on $fepA_{-173}$ mRNA in the presence of increasing concentrations of WT or mutant OmrA or OmrY sRNAs (A) or of a fixed concentration of OmrA(mut) and increasing amounts of purified Hfq (B). "Toeprint" and "duplex" indicate RT stops due to 30S/initiator tRNA binding to mRNA or to pairing of the sRNA, respectively. Full-size gel of (A) is shown in Figure S2A and Figure S2B shows a repeat of this experiment including OmrB and OmrBmut sRNAs.

(C) Design of the As28.43 DNA mimicking the Omr 5′ end interacting with *fepA* mRNA. The sequence of this AsDNA is based on the Omr nucleotides highlighted in gray, modified in order to have only Watson-Crick base pairs in the mRNA-AsDNA duplex. The same mutation as that introduced in the Omr 5′ end was introduced in As28.43.

(D) Toeprinting assay on $fepA_{-173}$ transcript in the presence of increasing concentrations of WT or mutant As28.43 AsDNA. In (A), (B), and (D), numbers above the gels indicate the ratio of the sRNA, hexameric Hfq, or AsDNA over the *fepA* mRNA. Full-size gels of (B) and (D) are shown in Figures S2C and S2D, respectively.

The RBS Is Not the Only *fepA* mRNA Region whose Accessibility Affects Ribosome Binding

Using an antisense scanning approach, it was shown previously that, for several *Salmonella* mRNAs, the ability of AsDNAs to compete with ribosome binding was lost when pairing occurred downstream of nucleotide +14 of the ORF (Bouvier et al., 2008). We therefore performed a similar antisense scanning experiment on the $fepA_{-173}$ transcript to determine whether the *fepA* ORF displays a specific sensitivity to AsDNAs binding, as suggested by the effect of As28.43. In this experiment, the toeprint signal on *fepA* mRNA was monitored in the presence of 20 different AsDNAs, perfectly complementary to the early *fepA* ORF with similar melting temperatures and whose 3′ ends were consecutively shifted by 2 nt (Figure 4A). A first group of AsDNAs (As−1.16 to As12.26) strongly inhibited toeprint, in agreement with the fact that they bind to *fepA* RBS (Figures 4B and 4C). In contrast, the three next AsDNAs, As14.27 to As18.31, base pair mostly downstream of the region bound by the 30S ribosomal subunit during translation initiation and, similar to what was observed previously (Bouvier et al., 2008), no longer inhibited toeprint formation. Surprisingly, however, the eight following scanning AsDNAs, As20.33 to As34.49 (group 2), recovered the ability to inhibit the toeprint, even though they base pair outside of the RBS (Figure 4). It is worth noting that binding of the various AsDNAs to *fepA* mRNA induced RT arrests of variable intensities downstream of the toeprint position, which in theory could induce a decrease in the toeprint signal by blocking RT progression. However, our experimental data seem to exclude this possibility: the last two scanning oligos, As36.52 and As38.53, induce strong RT stops at positions +45 and +46 but do not inhibit toeprint formation. This strongly suggests that the effect of As20.33 to As28.43 on the toeprint is not due to the blocking of RT as those AsDNAs induce weaker RT stops. Even though the use of AsDNAs is artificial, these data led us to consider that the *fepA* mRNA displays two distinct regions that positively impact the binding of the 30S subunit. The first corresponds to the RBS, and the second, which is more surprising, to the region extending from nucleotides 20 to 35 of *fepA* ORF. Interestingly, this second region partially overlaps but is not restricted to the OmrA/B binding site. Furthermore, a secondary structure prediction proposes the existence of an imperfect SL structure within the *fepA* ORF from nucleotides 19 to 46 (Figure 5A), opening the possibility that the group 2 AsDNAs, as OmrA/B, might inhibit toeprint formation via disruption of this structure.

The *fepA* Region Targeted by OmrA/B Forms a Stem-Loop Structure that Is Required for Control by These sRNAs

To provide experimental support for the predicted SL, we performed a structural probing analysis of the $fepA_{-26}$ transcript extending from nucleotides −26 to +129 *in vitro* using the chemical probes DMS (that modifies adenosine and to a lesser extent cytosine residues) and CMCT (that modifies guanosine and uridine residues). As shown in Figure 5A, most of the nucleotides located in the TIR of *fepA* displayed a moderate to strong reactivity toward the probes, suggesting that this region of *fepA* mRNA is mostly unstructured. In contrast, most nucleotides between positions +19 and +46 were poorly reactive, except for nucleotides 28–32 and 37–41, corresponding to the loop and bulge of the predicted SL. The structural probing data thus strongly support the existence of this SL. Because it encompasses the OmrA/B binding site, these results also suggest that control of *fepA* expression by these sRNAs would rely on disruption of this secondary structure.

This was more directly assessed by following repression by OmrA/B of a *fepA-lacZ* fusion, where formation of the SL was

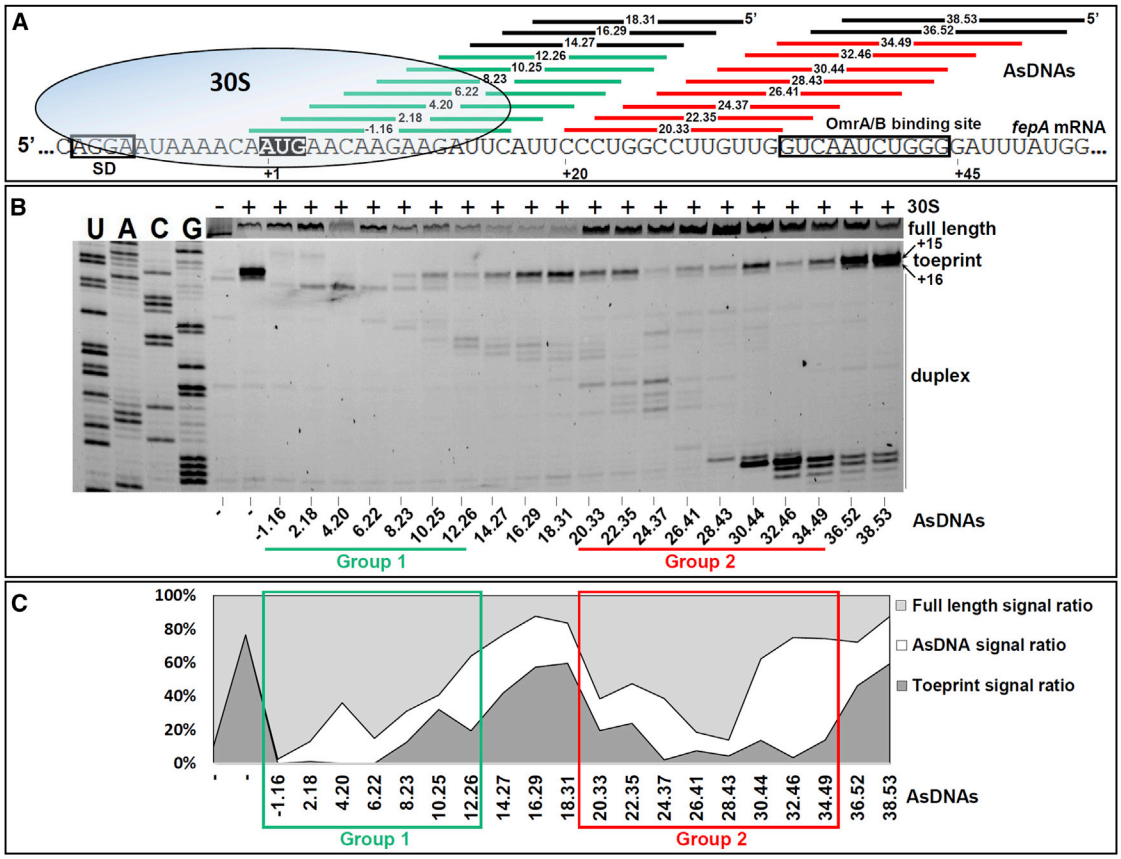

Figure 4. Formation of the *fepA* Translation Initiation Complex Depends on the Accessibility of Two Distinct Regions of the mRNA

(A) Schematic of the different oligonucleotides (AsDNAs) used in the antisense-scanning experiment. AsDNAs that inhibit the toeprint signal are indicated in color and those that do not are in black, respectively. The expected position of the 30S subunit on *fepA* mRNA in the translation initiation complex is shown schematically, together with the *fepA* SD sequence, AUG, and the minimal OmrA/B binding site identified in Figure 1.

(B) Toeprinting assay on $fepA_{-173}$ transcript in presence of the various AsDNAs in a 10-fold molar excess over the mRNA. The corresponding full-size gel is shown in Figure S3.

(C) Quantification of the toeprinting assay shown in (B). The sum of the full-length, toeprint, and AsDNA signals was set up at 100% for each lane. Hence, the toeprint is represented here as a percentage of total lane signals.

impaired by changing nucleotides +20 to +27 from CCCUGGCC to GGGAAAAA (G3A5 mutation in Figure 5B). The ability of the Omr to repress this mutant version of *fepA-lacZ* was strongly reduced: OmrA and OmrB repressed its expression by 2.2- and 1.6-fold, respectively, while they repressed expression of the WT fusion by 7.6- and 4.4-fold (Figure 5C). Because pairing of OmrA/B to nucleotides 20–27 of the *fepA* ORF is not required for control (Figure 1), the effect of the G3A5 mutant is most likely due to its preventing formation of the SL. In contrast, changing nucleotides +28 to +32 in the loop from UUGUU to AACAA (loop mutation in Figure 5B) did not affect the ability of OmrA/B to control *fepA* (repression factors of 9.4- and 5-fold, respectively; Figure 5C). This result indicates that pairing of the OmrA/B downstream of nucleotide +32 of *fepA* ORF is sufficient for the control, confirming the primary role of the Omr 5′ end in this interaction.

It is striking that several of the *fepA* nucleotides that pair to OmrA/B are located in the bulge, and we wondered whether this was a requisite for the control. We thus engineered a mutant version of the *fepA-lacZ* fusion, where 6 extra nt (AGGAUU), 5 of which being perfectly complementary to the bulged nucleotides, have been inserted in the 5′ strand of the SL (Figure 5B). In this "antiBulge" mutant, all nucleotides of the Omr pairing region are thus expected to pair with nucleotides from the 5′ strand, and interestingly, control by OmrA/B was completely abolished (Figure 5C). These data are not only consistent with the formation of the SL, but they also strongly suggest that the bulge is required for allowing the Omr 5′ end to interact with *fepA* mRNA, possibly serving as an anchor point for the sRNAs.

The Stem-Loop Activates FepA Synthesis in a Sequence-Independent Manner

Because OmrA/B likely inhibit *fepA* translation by disrupting the SL, we next investigated the role of this structure in *fepA* expression. For this purpose, the effect of diverse mutations on *fepA* expression was analyzed in the context of both the short and the long fusions described earlier. A first group of mutants consisted of changes of 5 or 8 nt on either side of the stem (mutants

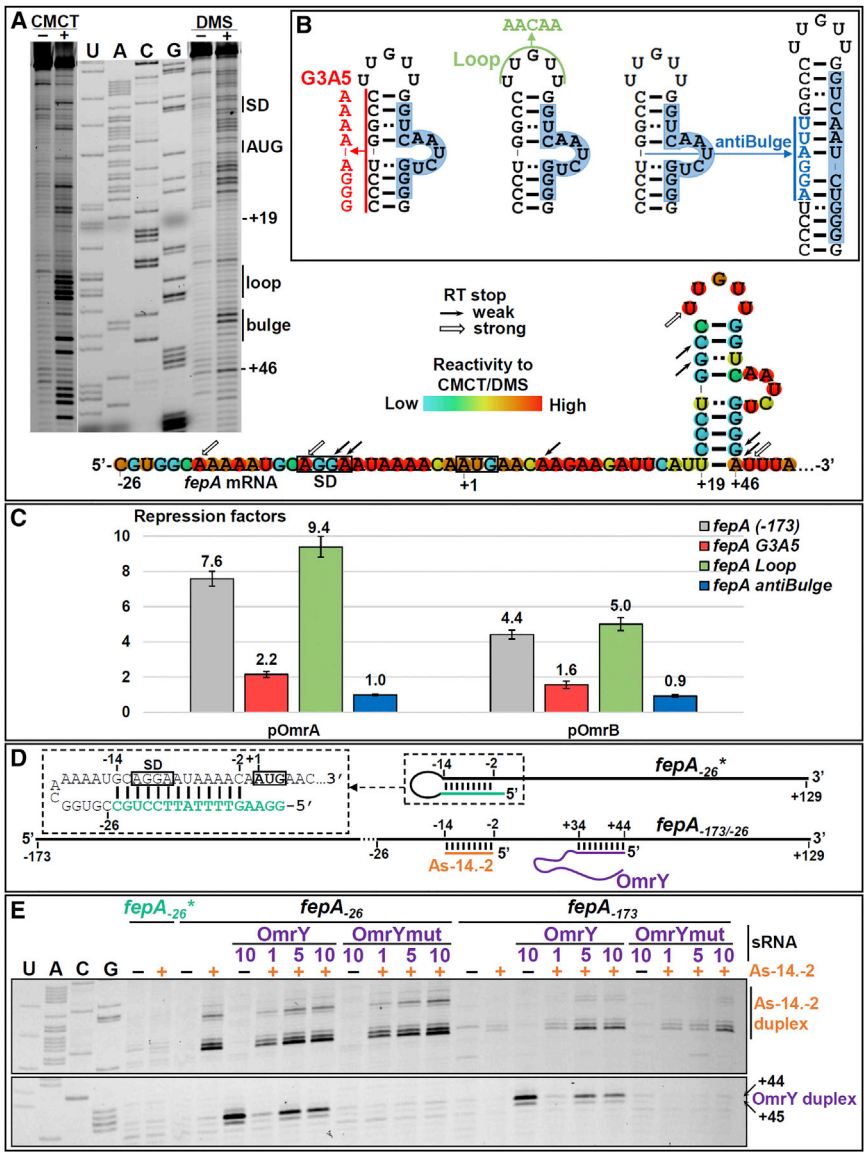

Figure 5. Regulation by OmrA/B Relies on the Disruption of a Secondary Structure in *fepA* mRNA, which Does Not Modify RBS Accessibility

(A) *In vitro* chemical probing assay of the secondary structure of the *fepA*$_{-26}$ transcript using CMCT and DMS. Stronger RT stops in the presence of the probe (+) than in its absence (–) indicate accessible nucleotides, which are therefore considered as unfolded. Positions relative to *fepA* start codon are indicated to the right of the gel. The full-size gel is reproduced in Figure S4A. A model of the secondary structure of the 5′ region of *fepA*$_{-26}$ derived from probing is shown. Nucleotides are colored according to their reactivity to DMS or CMCT, while arrows indicate RT stops that are not probe dependent.

(B) Mutations designed to disrupt the predicted secondary structure (G3A5), to alter the sequence of the loop (Loop), or to pair all nucleotides of the OmrA/B binding site to nucleotides of the 5′ strand of the SL (antiBulge). The base pair at the base of the SL (U-A in *fepA* mRNA and U-G in *fepA-lacZ*) is omitted in this representation. Nucleotides highlighted in blue indicate the minimal Omr binding site as defined in Figure 1.

(C) Repression by OmrA or OmrB of the *fepA*$_{-173}$-*lacZ* fusion, WT or carrying the G3A5, Loop, or antiBulge mutation. Strains used in this experiment are JJ0015, JJ0286, JJ0281, and MG2247; raw data used to calculate the repression factors are given in Figure S4B.

(D) Principle of the RT experiment performed to assess the *fepA* mRNA RBS accessibility: following duplex formation between OmrY or OmrYmut and either *fepA*$_{-26}$ *or fepA*$_{-173}$ transcript, binding of the As−14.−2 AsDNA to the transcripts was analyzed by RT. The construct *fepA*$_{-26}$* is a modification of *fepA*$_{-26}$ carrying 16 extra nucleotides at the 5′ end that can form a secondary structure occluding the SD region.

(E) Selected portions of the gel analyzing the RT products. Upper and lower panels show the RT stops due to As−14.−2 binding and to OmrY-*fepA* mRNA duplex formation, respectively. The full gel is shown in Figure S5.

A5, U5, G3A5, and U5C3 in Figure 6A), which should impair formation of the SL. All four mutants decreased expression of both the short and the long *fepA-lacZ* fusions, with a stronger effect observed for the 8 nt changes (Figure 6B). These changes were then combined to re-establish the SL structure (mutants Comp1 and Comp2; Figure 6A), which restored, at least partially, a higher *fepA* expression. In the case of the Comp1 change in the short fusion, the restoration of *fepA* expression was essentially complete (Figure 6B). These effects were independent of the Omr sRNAs as the same results were obtained in strains deleted for *omrAB* (Figure S6A). These data strongly suggest that formation of the SL promotes FepA synthesis. Furthermore, as *fepA* expression was also increased with the Comp1 and Comp2 constructs, where most of the pairing nucleotides of the SL have been changed, it appears that this effect is largely sequence independent. The fact that the Comp2 change is not as efficient as Comp1 in restoring *fepA* expression could be due to a slight difference in the topology and/or the stability of the Comp2 SL compared to the WT structure.

The functional importance of the unpaired nucleotides of the SL was then assayed by either deleting the bulged nucleotides (mutant Δbulge in Figure 6A) or using the Loop mutant (Figure 5B). Neither of these mutations had a strong impact on *fepA* expression (Figure 6B). Furthermore, formation of the SL still activated *fepA* expression in those two constructs as shown by the fact that the Loop mutant fusion was controlled by the Omr sRNAs similarly to the WT fusion (Figure 5C) and that expression of the Δbulge construct was weakened by the G3A5 change to the same extent as the WT (Figure 6E). Together, these data strongly suggest that the SL activates *fepA* expression via its secondary rather than primary structure and that changes in the topology of this structure (e.g., by deleting the bulge) are permissible. Importantly, the G3A5, U5C3, Loop, and Δbulge mutants show that all nucleotides can be modified without interfering with the

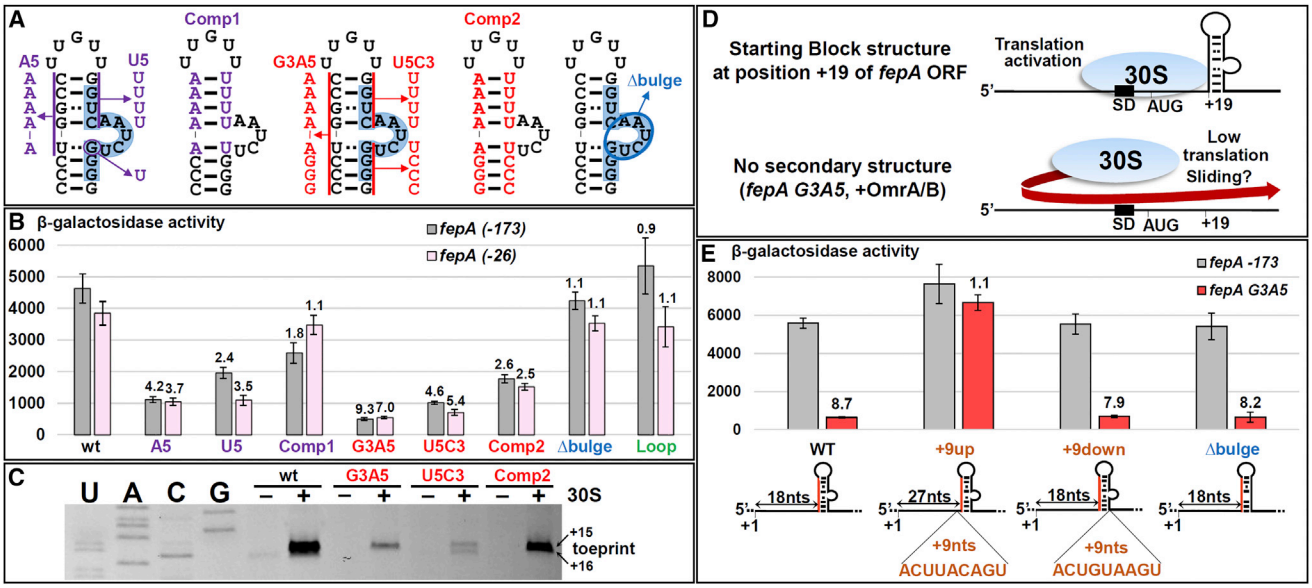

Figure 6. The *fepA* mRNA Stem-Loop Structure Activates Translation in a Sequence-Independent Manner, Possibly by Acting as a "Starting Block" Structure

(A) Mutations designed to alter (mutants A5, U5, G3A5, and U5C3) or restore (mutants Comp1 and Comp2) the SL structure. The Δbulge mutant consists in the deletion of nucleotides 37–42. The Loop mutant is depicted in Figure 5B. The minimal OmrA/B binding site as defined in Figure 1 is highlighted in blue.

(B) β-galactosidase activity of strains carrying these different versions of the $fepA_{-173}$-*lacZ* or the $fepA_{-26}$-*lacZ* fusion. Strains used in this experiment are, from left to right, MG1772, JJ0150, JJ0225, JJ0190, JJ0233, JJ0229, JJ0237, JJ0241, and JJ0192 for the $fepA_{-173}$-*lacZ* variants and JJ0135, JJ0120, JJ0227, JJ0180, JJ0235, JJ0231, JJ0238, JJ0243, and JJ0193 for the $fepA_{-26}$-*lacZ* variants. Ratios between activities of the WT and each mutant fusion are given above the bars.

(C) Toeprinting assay on $fepA_{-173}$ mutant transcripts. Only the portion of the gel with the toeprint signal is shown; full-size gel is reproduced in Figure S6B.

(D) Model of the starting block mechanism: the SL at position +19 of *fepA* mRNA would arrest scanning of the 30S ribosomal subunit at the proper position to initiate translation. Disruption of the SL by the Omr sRNAs or by the G3A5 mutation decreases translation initiation, possibly because of sliding of the 30S subunit on *fepA* mRNA.

(E) Activation of *fepA* expression by the SL structure was determined after insertion of 9 nt upstream (mutant +9up) or downstream (mutant +9down) of the SL, as well as in the Δbulge variant. The activation factor, given above the red bars, is the ratio of the β-galactosidase activity of the WT SL fusion (gray bars) over the activity of the G3A5 derivative (red bars). Strains used in this experiment are, from left to right, MG1772, JJ0268, JJ0271, and JJ0241 for the WT derivatives and JJ0233, JJ0250, JJ0260, and JJ0290 for the G3A5 mutants.

activating role of this structure, arguing strongly against a structural switch that would occur upon OmrA/B binding and that would ultimately affect RBS accessibility.

We nonetheless wanted to more directly assess whether binding of the Omr 5′ end would affect *fepA* RBS accessibility. For this purpose, we first repeated the probing experiment of *fepA* mRNA (Figure 5A) in the presence of an excess of OmrA or OmrY sRNA but found that both sRNAs fail to bind to *fepA* mRNA in this experiment (Figure S4A). This is different from what we observed in other *in vitro* experiments, such as the toeprinting assays (see, for example, Figure 3), and this is most likely due to the use of different buffers required for DMS- or CMCT-induced modifications. To assess RBS accessibility, we thus chose instead to follow the binding of the As−14.−2 AsDNA to *fepA* mRNA in an RT experiment (Figure 5D). Because As−14.−2 is perfectly complementary to nucleotides −14 to −2 of *fepA*, which encompass the SD sequence, its binding is expected to reflect the accessibility of the SD region. As a proof of principle, we first showed that this was indeed the case: while strong RT stops indicated As−14.−2 binding to $fepA_{-26}$ or $fepA_{-173}$ transcripts, no stop was detected when we used instead a $fepA_{-26}^{*}$ transcript carrying an extra sequence at its 5′ end that can occlude the SD region. Binding of As−14.−2 was then analyzed on $fepA_{-26}$ or $fepA_{-173}$ transcripts that were beforehand denatured and renatured in the presence of increasing concentrations of OmrY or OmrYmut sRNA. As visible on Figure 5E, the specific binding of OmrY had no noticeable effect on As−14.−2 binding to *fepA* mRNA, providing yet another indication that control of *fepA* by OmrA/B does not rely on a change in RBS accessibility.

The Stem-Loop Structure Acts at the Translation Initiation Level

Our *in vivo* results did not allow us to discriminate between an effect of the SL on *fepA* mRNA translation, stability, processing, or yet another process. However, because disruption of this SL by OmrA/B sRNAs (or group 2 AsDNAs) inhibited 30S ribosomal subunit binding to *fepA* mRNA, it seemed likely that it acted at the translation initiation step. This was tested *in vitro* by performing a toeprinting assay using the WT $fepA_{-173}$ transcript or its variants G3A5, U5C3, or Comp2. The results were in remarkable agreement with what was observed *in vivo* with the fusions: disruption of the SL using the G3A5 or U5C3 mutations strongly inhibited the toeprint, while restoring the structure

using the compensatory change partially recovered the toeprint signal (Figure 6C). This demonstrates that the SL enhances the formation of the ternary translation initiation complex without requiring other actors than the *fepA* transcript, the 30S ribosomal subunit, and the initiator tRNA.

How Could This Structure Activate Translation of *fepA* mRNA?

An intriguing question raised by our results is the mechanism by which the SL activates translation initiation at such an early step. One possibility is that it would do so by helping to recruit the 30S ribosomal subunit. This could be due, for instance, to an interaction between the SL and one of the 30S components (protein or RNA). Importantly, however, the effect of this SL is independent of its nucleotide sequence and is permissive to topological changes. This is hard to reconcile with a recruitment model at first sight; nonetheless, ribosomal proteins tend to interact with the sugar-phosphate backbone on ribosomal RNA (Brodersen et al., 2002; Mangeol et al., 2011), and similar interactions could occur between proteins and the activating SL. Other elements of the *fepA* mRNA could furthermore be involved in the activating role of the SL and provide specificity.

Alternatively, one might envision that this structure activates translation initiation by providing a "starting block" to the 30S subunit (Figure 6D). In this regard, it is striking that the 5′ edge of the SL is located at position +19 of *fepA* ORF, exactly contiguous to the 3′ edge of the RBS (Hüttenhofer and Noller, 1994). It would thus be ideally located to block the 30S subunit at proper position for an efficient translation initiation. Results of Figure 5E suggested that the *fepA* SD sequence is as accessible in the absence as in the presence of the SL. This is consistent with the affinity between the 30S ribosomal subunit and the *fepA* mRNA being similar regardless of the formation of the SL. If so, the increase in the toeprint signal observed in presence of the SL (Figure 6C) could rely on a "starting block" mechanism (Figure 6D) through which the SL would block the 30S ribosomal subunit from sliding on the mRNA without establishing a translation initiation complex. This optimized positioning of the 30S subunit would ultimately lead to an increased translation initiation rate. A prediction of this starting block model is that increasing the distance between the *fepA* start codon and the SL should prevent the ability of the latter to activate translation. This was tested by measuring the activation by the SL when 9 extra nt were introduced after position +18 (mutant +9up in Figure 6E). While the SL activated *fepA* expression by almost 10-fold when located at nucleotide +19, i.e., in the WT situation, activation was completely abolished when it was moved to position +28 (Figure 6E). In contrast, the SL still activated *fepA* expression by 7.5-fold when 9 nt were introduced after nucleotide +45, i.e., downstream of this structure (mutant +9down, Figure 6E). Together, these results indicate that the distance between the start codon and the SL is important for the ability of this structure to activate translation. Even though this does not necessarily rule out the recruitment model, this is in perfect agreement with the starting block hypothesis. Thus, at least in the *fepA* context, translation initiation is activated by the presence of a SL that may help the correct positioning of the 30S ribosomal subunit for efficient initiation.

A Similar Activating Role for a Stem-Loop in *bamA* mRNA

Another obvious question raised by our results is whether translation activation by a SL is restricted to *fepA* or is, in contrast, a more general phenomenon. To address this, we searched for putative SL located around the nucleotide +20 in a subset of diverse mRNAs by combining Mfold prediction (Zuker, 2003) and visual inspection and found that such SL can be predicted in many mRNAs (a few examples are given in Figure 7A). One of the most convincing SLs is predicted within *bamA*, encoding an essential component of the Bam complex that allows the insertion of β-barrel integral OMPs in the outer membrane of Gram-negative bacteria (Ricci and Silhavy, 2012). Another striking feature of the *bamA* mRNA is that it possesses a putative AGGA SD sequence located 16 nt upstream of the AUG (a distance conserved in several bacteria; Figure S7A), i.e., a spacing that is not optimal for efficient initiation, and whether it is really involved in the initial binding of the ribosome can be questioned. We experimentally tested whether this predicted SL could have a role in *bamA* expression, both *in vivo* using compensatory changes introduced in a *bamA-lacZ* translational fusion and *in vitro* by a toeprinting assay (Figures 7B–7D). The results are in all points similar to those obtained with *fepA*. First, mutations Mut5′ and Mut3′ that are expected to disrupt the SL strongly decreased expression of the fusion, which was restored to its WT level in presence of the compensatory change (Comp) (Figure 7C). These data support both the existence of the predicted SL and its positive role in *bamA* expression. Furthermore, formation of the translation initiation complex was detected by toeprinting for both the WT and the Comp version of *bamA*, but not for the Mut5′ and Mut3′ variants, showing that, as for *fepA*, the SL promotes translation initiation at a very early stage (Figure 7D).

Importantly, while *fepA* is found only in enterobacteria, the *bamA* gene is present in much more phylogenetically distant bacteria, and despite important variations at the nucleotide sequence level, a similar SL can be predicted in *bamA* mRNA of other γ-proteobacteria such as *Vibrio* species (Figure S7). This suggests that this novel mechanism of translation activation by a SL is conserved in a wide set of Gram-negative bacteria.

DISCUSSION

A Role for mRNA Secondary Structures in Activating Translation

In bacteria, several *cis*-acting elements embedded in the mRNA are known to play important roles in translation, at either the sequence or the structure level. The most obvious example is the evolutionary conserved SD sequence, but in addition, several enhancers that improve binding of the 30S subunit, such as (A) CA-rich motifs (Sharma et al., 2007; Yang et al., 2014) or A-rich regions in the mRNA (Brock et al., 2007), have been described.

Secondary structures in mRNA are known to impact translation as well because they represent thermodynamic and kinetic barriers that must be disrupted to allow the ribosome to bind to or move on mRNA. Secondary structures have been reported to negatively affect translation initiation by decreasing access of the ribosome to the RBS, for instance (de Smit and van Duin, 1990), or by slowing down the elongation rate of the translating ribosome (e.g., Qu et al., 2011; Wen et al., 2008).

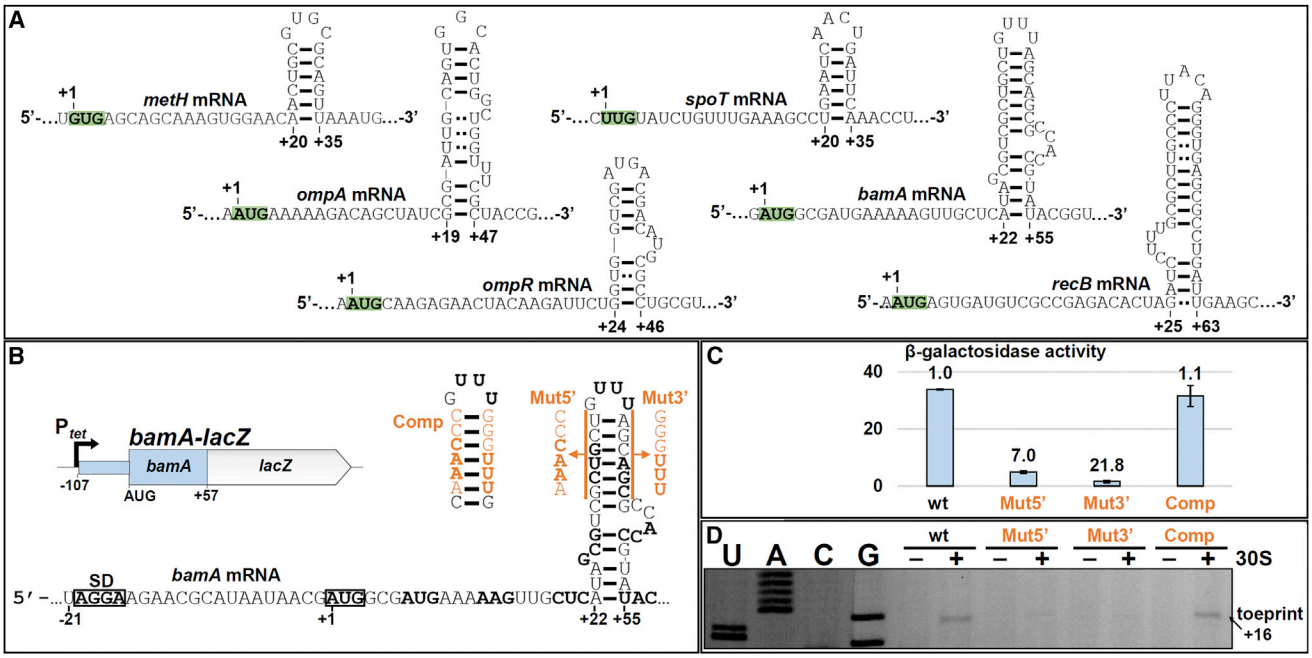

Figure 7. A Similar Activating Stem-Loop Structure in the *bamA* mRNA

(A) Examples of SL predicted in a subset of *E. coli* mRNAs around the position +20 of the ORF. The start codon is indicated by a green square in each mRNA. Sequences between nucleotide −25 and the start codon are given in Figure S6C.

(B) Scheme of the P_{tet}-*bamA-lacZ* fusion and of the mutations introduced in the SL to assay its role in *bamA* expression.

(C) β-galactosidase activities of the different *bamA-lacZ* fusions. Strains used in this experiment are JJ0383 (WT), JJ0384 (Mut5′), JJ0385 (Mut3′), and JJ0386 (Comp). Ratios between activities of the WT and each mutant fusion are given above the bars.

(D) Toeprinting assay on WT and mutant *bamA* mRNA fragments. Only the portion of the gel with the toeprint signal is shown; full-size gel is reproduced in Figure S6D.

The present work shows that mRNA secondary structures located around position +20 can surprisingly promote formation of the ternary initiation complex and thus activate translation, possibly by helping to correctly position the 30S ribosomal subunit for optimal translation initiation. Why would some mRNAs require such a SL for maximal expression? In the case of *bamA*, it is tempting to speculate that this is related to the unusually long SD-AUG spacing. Regarding *fepA*, the involvement of such an activating SL in translation is more puzzling at first sight given the canonical AGGA SD sequence optimally spaced from the start codon (8 nt). This could suggest that *cis*-elements of this mRNA somehow destabilize its interaction with the 30S ribosomal subunit. In line with this, we found that, when introduced at nucleotide +20 of a different mRNA, this SL no longer activated translation, indicating that its effect depends on specific features of the *fepA* mRNA (unpublished data). Because the SL activates expression of the short *fepA-lacZ* fusion (Figure 6), these specific features are most likely located between nucleotides −26 and +18 of *fepA* mRNA, and it will be interesting to determine how they participate in *fepA* expression and its control by the SL.

Folding of the Activating Stem-Loop Structure and Translation

The activating SL identified in *fepA* and *bamA* mRNAs are part of ORF and are thus disrupted by translating ribosomes. Considering that disruption of the SL significantly decreases the toeprint signal on those mRNAs (Figures 6 and 7), we can assume that each translating ribosome will transiently decrease the initiation rate until the hairpin refolds. Given that the time needed to form a simple hairpin helix is less than 1 ms *in vitro* (Crothers et al., 1974), while initiation frequency for a well-translated gene like *lacZ* is on the second range (Kennell and Riezman, 1977), it is likely that the SL refolds after clearance of the translating ribosome and before binding of the next ribosome. Therefore, activation of ribosome binding by this SL can affect several rounds of translation and might ensure that translation is kept within a given range.

Are Activating Stem-Loops a General Feature of mRNAs?

In addition to the *fepA* and *bamA* genes, it is likely that such activating SLs are present in other genes given that they can be predicted around position +20 in yet more *E. coli* mRNAs (a few are shown in Figure 7A). Also, in line with the idea that our findings could apply to mRNAs other than *fepA* or *bamA*, it was previously reported that introduction of a 7 bp SL at position +19 dramatically enhanced the translation of poorly expressed heterologous genes (Paulus et al., 2004). Furthermore, the analysis of *fepA* sequences from diverse enterobacteria and of *bamA* in several γ-proteobacteria

indicates that these structures are likely to be conserved in several species despite changes in the nucleotide and possibly in the amino acid sequence (Figure S7), suggesting that translation activation by SL structures occurs in these organisms as well.

Nonetheless, data from recent genome-wide studies of RNA structures in *E. coli* did not specifically point out the existence of secondary structures near the position +20 of mRNAs (Burkhardt et al., 2017; Del Campo et al., 2015). And, as mentioned above, the ability of the *fepA* SL to activate translation does not necessarily withstand a change in the surrounding mRNA sequence. Thus, translation activation by SL might be limited to a subset of mRNAs, whose identity remains to be deciphered.

The Activating Stem-Loop as a Target for Regulators of *fepA*

We have identified at least two regulators that modulate *fepA* expression by targeting this activating SL. These regulators are the OmrA and OmrB sRNAs, whose binding site on *fepA* mRNA corresponds to the 3′ side of the SL and, accordingly, repress FepA synthesis at the translation level. It is tempting to speculate that yet other post-transcriptional regulators, being sRNAs or proteins, could target this structure in *fepA* or *bamA*. In addition, these SLs could also form thermosensors and integrate the temperature as an additional cue of FepA or BamA synthesis.

From a physiological standpoint, regulating *fepA* expression at the post-transcriptional level, by OmrA/B or other regulators, is expected to change FepA levels in response to different environmental cues and with different dynamic properties than the well-established transcriptional control by the Fur repressor. However, one can wonder what would be the advantage of limiting FepA synthesis by OmrA/B sRNAs that themselves respond to the EnvZ-OmpR TCS or to the RpoS sigma factor (at least for OmrA). A possible connection lies in the fact that EnvZ-OmpR is activated in response to acid stress (Quinn et al., 2014; Stincone et al., 2011), i.e., conditions that increase the solubility of iron. OmrA/B can thus participate in limiting not only the levels of FepA, but also of other receptors of iron-siderophore complexes, such as FecA or CirA, under those conditions where iron scavenging by siderophores might be less needed, or even possibly harmful. Another important note is that both OmrA and OmrB are induced upon host infection (Westermann et al., 2016). Because FepA and other iron-dependent OMPs are recognized by the host immune system (Fernandez-Beros et al., 1989), decreasing their levels in response to the infectious process may help to limit the host response to bacterial infection.

Together with previous reports, the study presented here highlights the wide diversity in the mRNA regions targeted by sRNAs and in the regulatory mechanisms by which sRNAs control gene expression. Importantly, it also led to the identification of translation-activating SLs that promote formation of the initiation ternary complex on several bacterial mRNAs, suggesting that the definition of RBS may need to be reevaluated for some transcripts.

STAR★METHODS

Detailed methods are provided in the online version of this paper and include the following:

- KEY RESOURCES TABLE
- CONTACT FOR REAGENT AND RESOURCE SHARING
- EXPERIMENTAL MODEL AND SUBJECT DETAILS
  - Bacterial Strains
- METHOD DETAILS
  - Oligonucleotides and Plasmids
  - β-galactosidase Assays
  - RNA Extraction and Northern Blot Assays
  - Protein Extraction and Western Blot Assays
  - *In Vitro* RNA Transcription
  - *In Vitro* Reverse Transcription
  - *In Vitro* Toeprinting and RNA Structure Probing Assays
  - *In Vitro* RNA Structure Probing
- QUANTIFICATION AND STATISTICAL ANALYSIS

SUPPLEMENTAL INFORMATION

Supplemental Information includes seven figures and two tables and can be found with this article online at http://dx.doi.org/10.1016/j.molcel.2017.08.015.

AUTHOR CONTRIBUTIONS

M.G. and J.J. designed research; J.J. performed experiments; M.G., J.J., and C.C. analyzed and interpreted the data and wrote the paper.

ACKNOWLEDGMENTS

We are grateful to Kathleen Postle and Knud Nierhaus for providing us the FepA or the S1 antibody, respectively, and to Eliane Hajnsdorf for the gift of purified Hfq. We thank Audrey Coornaert for preliminary work during her M2 internship and Mathias Springer and Ciaran Condon for insightful comments on the manuscript. This work was supported by the CNRS, the ANR (grant ANR-14-CE10-0004-01 to M.G.), and the "Initiative d'Excellence" program from the French State (Grant "DYNAMO," ANR-11-LABX-0011). J.J. is a recipient of a DYNAMO PhD fellowship.

Received: February 27, 2017
Revised: June 8, 2017
Accepted: August 18, 2017
Published: September 14, 2017

REFERENCES

Balbontín, R., Villagra, N., Pardos de la Gándara, M., Mora, G., Figueroa-Bossi, N., and Bossi, L. (2016). Expression of IroN, the salmochelin siderophore receptor, requires mRNA activation by RyhB small RNA homologues. Mol. Microbiol. *100*, 139–155.

Bandyra, K.J., Said, N., Pfeiffer, V., Górna, M.W., Vogel, J., and Luisi, B.F. (2012). The seed region of a small RNA drives the controlled destruction of the target mRNA by the endoribonuclease RNase E. Mol. Cell *47*, 943–953.

Bouvier, M., Sharma, C.M., Mika, F., Nierhaus, K.H., and Vogel, J. (2008). Small RNA binding to 5′ mRNA coding region inhibits translational initiation. Mol. Cell *32*, 827–837.

Brock, J.E., Paz, R.L., Cottle, P., and Janssen, G.R. (2007). Naturally occurring adenines within mRNA coding sequences affect ribosome binding and expression in *Escherichia coli*. J. Bacteriol. *189*, 501–510.

Brodersen, D.E., Clemons, W.M., Jr., Carter, A.P., Wimberly, B.T., and Ramakrishnan, V. (2002). Crystal structure of the 30 S ribosomal subunit from *Thermus thermophilus*: structure of the proteins and their interactions with 16 S RNA. J. Mol. Biol. *316*, 725–768.

Brosse, A., Korobeinikova, A., Gottesman, S., and Guillier, M. (2016). Unexpected properties of sRNA promoters allow feedback control via regulation of a two-component system. Nucleic Acids Res. *44*, 9650–9666.

Burkhardt, D.H., Rouskin, S., Zhang, Y., Li, G.-W., Weissman, J.S., and Gross, C.A. (2017). Operon mRNAs are organized into ORF-centric structures that predict translation efficiency. eLife *6*, e22037.

Coornaert, A., Chiaruttini, C., Springer, M., and Guillier, M. (2013). Post-transcriptional control of the *Escherichia coli* PhoQ-PhoP two-component system by multiple sRNAs involves a novel pairing region of GcvB. PLoS Genet. *9*, e1003156.

Crothers, D.M., Cole, P.E., Hilbers, C.W., and Shulman, R.G. (1974). The molecular mechanism of thermal unfolding of *Escherichia coli* formylmethionine transfer RNA. J. Mol. Biol. *87*, 63–88.

Darfeuille, F., Unoson, C., Vogel, J., and Wagner, E.G. (2007). An antisense RNA inhibits translation by competing with standby ribosomes. Mol. Cell *26*, 381–392.

De Lay, N., and Gottesman, S. (2012). A complex network of small non-coding RNAs regulate motility in *Escherichia coli*. Mol. Microbiol. *86*, 524–538.

de Smit, M.H., and van Duin, J. (1990). Secondary structure of the ribosome binding site determines translational efficiency: a quantitative analysis. Proc. Natl. Acad. Sci. USA *87*, 7668–7672.

Del Campo, C., Bartholomäus, A., Fedyunin, I., and Ignatova, Z. (2015). Secondary structure across the bacterial transcriptome reveals versatile roles in mRNA regulation and function. PLoS Genet. *11*, e1005613.

Fernandez-Beros, M.E., Gonzalez, C., McIntosh, M.A., and Cabello, F.C. (1989). Immune response to the iron-deprivation-induced proteins of *Salmonella typhi* in typhoid fever. Infect. Immun. *57*, 1271–1275.

Guillier, M., and Gottesman, S. (2006). Remodelling of the *Escherichia coli* outer membrane by two small regulatory RNAs. Mol. Microbiol. *59*, 231–247.

Guillier, M., and Gottesman, S. (2008). The 5′ end of two redundant sRNAs is involved in the regulation of multiple targets, including their own regulator. Nucleic Acids Res. *36*, 6781–6794.

Heidrich, N., Moll, I., and Brantl, S. (2007). *In vitro* analysis of the interaction between the small RNA SR1 and its primary target *ahrC* mRNA. Nucleic Acids Res. *35*, 4331–4346.

Higgs, P.I., Larsen, R.A., and Postle, K. (2002). Quantification of known components of the *Escherichia coli* TonB energy transduction system: TonB, ExbB, ExbD and FepA. Mol. Microbiol. *44*, 271–281.

Holmqvist, E., Reimegård, J., Sterk, M., Grantcharova, N., Römling, U., and Wagner, E.G. (2010). Two antisense RNAs target the transcriptional regulator CsgD to inhibit curli synthesis. EMBO J. *29*, 1840–1850.

Hüttenhofer, A., and Noller, H.F. (1994). Footprinting mRNA-ribosome complexes with chemical probes. EMBO J. *13*, 3892–3901.

Jagodnik, J., Brosse, A., Le Lam, T.N., Chiaruttini, C., and Guillier, M. (2017). Mechanistic study of base-pairing small regulatory RNAs in bacteria. Methods *117*, 67–76.

Kawamoto, H., Koide, Y., Morita, T., and Aiba, H. (2006). Base-pairing requirement for RNA silencing by a bacterial small RNA and acceleration of duplex formation by Hfq. Mol. Microbiol. *61*, 1013–1022.

Kennell, D., and Riezman, H. (1977). Transcription and translation initiation frequencies of the *Escherichia coli lac* operon. J. Mol. Biol. *114*, 1–21.

Kery, M.B., Feldman, M., Livny, J., and Tjaden, B. (2014). TargetRNA2: identifying targets of small regulatory RNAs in bacteria. Nucleic Acids Res. *42*, W124-9.

Lévi-Meyrueis, C., Monteil, V., Sismeiro, O., Dillies, M.A., Monot, M., Jagla, B., Coppée, J.Y., Dupuy, B., and Norel, F. (2014). Expanding the RpoS/σS-network by RNA sequencing and identification of σS-controlled small RNAs in *Salmonella*. PLoS ONE *9*, e96918.

Mandin, P., and Gottesman, S. (2010). Integrating anaerobic/aerobic sensing and the general stress response through the ArcZ small RNA. EMBO J. *29*, 3094–3107.

Mangeol, P., Bizebard, T., Chiaruttini, C., Dreyfus, M., Springer, M., and Bockelmann, U. (2011). Probing ribosomal protein-RNA interactions with an external force. Proc. Natl. Acad. Sci. USA *108*, 18272–18276.

Massé, E., Escorcia, F.E., and Gottesman, S. (2003). Coupled degradation of a small regulatory RNA and its mRNA targets in *Escherichia coli*. Genes Dev. *17*, 2374–2383.

Miller, J.H. (1992). A Short Course in Bacterial Genetics (Cold Spring Harbor Laboratory Press).

Obana, N., Shirahama, Y., Abe, K., and Nakamura, K. (2010). Stabilization of *Clostridium perfringens* collagenase mRNA by VR-RNA-dependent cleavage in 5′ leader sequence. Mol. Microbiol. *77*, 1416–1428.

Papenfort, K., Sun, Y., Miyakoshi, M., Vanderpool, C.K., and Vogel, J. (2013). Small RNA-mediated activation of sugar phosphatase mRNA regulates glucose homeostasis. Cell *153*, 426–437.

Paulus, M., Haslbeck, M., and Watzele, M. (2004). RNA stem-loop enhanced expression of previously non-expressible genes. Nucleic Acids Res. *32*, e78.

Peano, C., Wolf, J., Demol, J., Rossi, E., Petiti, L., De Bellis, G., Geiselmann, J., Egli, T., Lacour, S., and Landini, P. (2015). Characterization of the *Escherichia coli* σ(S) core regulon by Chromatin Immunoprecipitation-sequencing (ChIP-seq) analysis. Sci. Rep. *5*, 10469.

Pfeiffer, V., Papenfort, K., Lucchini, S., Hinton, J.C., and Vogel, J. (2009). Coding sequence targeting by MicC RNA reveals bacterial mRNA silencing downstream of translational initiation. Nat. Struct. Mol. Biol. *16*, 840–846.

Qu, X., Wen, J.D., Lancaster, L., Noller, H.F., Bustamante, C., and Tinoco, I., Jr. (2011). The ribosome uses two active mechanisms to unwind messenger RNA during translation. Nature *475*, 118–121.

Quinn, H.J., Cameron, A.D., and Dorman, C.J. (2014). Bacterial regulon evolution: distinct responses and roles for the identical OmpR proteins of *Salmonella Typhimurium* and *Escherichia coli* in the acid stress response. PLoS Genet. *10*, e1004215.

Ramirez-Peña, E., Treviño, J., Liu, Z., Perez, N., and Sumby, P. (2010). The group A Streptococcus small regulatory RNA FasX enhances streptokinase activity by increasing the stability of the *ska* mRNA transcript. Mol. Microbiol. *78*, 1332–1347.

Ricci, D.P., and Silhavy, T.J. (2012). The Bam machine: a molecular cooper. Biochim. Biophys. Acta *1818*, 1067–1084.

Salvail, H., Caron, M.P., Bélanger, J., and Massé, E. (2013). Antagonistic functions between the RNA chaperone Hfq and an sRNA regulate sensitivity to the antibiotic colicin. EMBO J. *32*, 2764–2778.

Sharma, C.M., Darfeuille, F., Plantinga, T.H., and Vogel, J. (2007). A small RNA regulates multiple ABC transporter mRNAs by targeting C/A-rich elements inside and upstream of ribosome-binding sites. Genes Dev. *21*, 2804–2817.

Stincone, A., Daudi, N., Rahman, A.S., Antczak, P., Henderson, I., Cole, J., Johnson, M.D., Lund, P., and Falciani, F. (2011). A systems biology approach sheds new light on *Escherichia coli* acid resistance. Nucleic Acids Res. *39*, 7512–7528.

Vogel, J., and Luisi, B.F. (2011). Hfq and its constellation of RNA. Nat. Rev. Microbiol. *9*, 578–589.

Wagner, E.G., and Romby, P. (2015). Small RNAs in bacteria and archaea: who they are, what they do, and how they do it. Adv. Genet. *90*, 133–208.

Wen, J.D., Lancaster, L., Hodges, C., Zeri, A.C., Yoshimura, S.H., Noller, H.F., Bustamante, C., and Tinoco, I. (2008). Following translation by single ribosomes one codon at a time. Nature *452*, 598–603.

Westermann, A.J., Förstner, K.U., Amman, F., Barquist, L., Chao, Y., Schulte, L.N., Müller, L., Reinhardt, R., Stadler, P.F., and Vogel, J. (2016). Dual RNA-seq unveils noncoding RNA functions in host-pathogen interactions. Nature *529*, 496–501.

Wright, P.R., Georg, J., Mann, M., Sorescu, D.A., Richter, A.S., Lott, S., Kleinkauf, R., Hess, W.R., and Backofen, R. (2014). CopraRNA and IntaRNA: predicting small RNA targets, networks and interaction domains. Nucleic Acids Res. *42*, W119-23.

Yang, Q., Figueroa-Bossi, N., and Bossi, L. (2014). Translation enhancing ACA motifs and their silencing by a bacterial small regulatory RNA. PLoS Genet. *10*, e1004026.

Yusupova, G.Z., Yusupov, M.M., Cate, J.H., and Noller, H.F. (2001). The path of messenger RNA through the ribosome. Cell *106*, 233–241.

Zuker, M. (2003). Mfold web server for nucleic acid folding and hybridization prediction. Nucleic Acids Res. *31*, 3406–3415.

STAR★METHODS

KEY RESOURCES TABLE

REAGENT or RESOURCE	SOURCE	IDENTIFIER
Antibodies		
Rabbit polyclonal anti-FepA	K. Postle; Higgs et al., 2002	N/A
Rabbit polyclonal anti-S1	K. Nierhaus	N/A
Bacterial and Virus Strains		
Escherichia coli K-12 MG1655 strain	F. Blattner	RefSeq NC000913.3
Strains used in this study all derive from MG1655 and are listed in Table S1	This study or references in Table S1	N/A
Chemicals, Peptides, and Recombinant Proteins		
DMS	Sigma-Aldrich	Cat#D186309
CMCT	Sigma-Aldrich	Cat#C106402
Oligonucleotides		
All oligonucleotides used in this study are listed in Table S2	This study	N/A
Recombinant DNA		
Plasmids pBRplac, pBRplacOmrA, pBRplacOmrB	Guillier and Gottesman, 2006	N/A
Plasmids pBRplacOmrAmut, pBRplacOmrBmut, pBRplacOmrY, and pBRplacOmrYmut	This study	N/A
Software and Algorithms		
MFold	Zuker, 2003	http://unafold.rna.albany.edu/?q=mfold/RNA-Folding-Form
ImageJ	ImageJ freeware	https://imagej.nih.gov/ij/

CONTACT FOR REAGENT AND RESOURCE SHARING

Further information and requests for resources and reagents should be directed to and will be fulfilled by the Lead Contact, Maude Guillier (maude.guillier@ibpc.fr).

EXPERIMENTAL MODEL AND SUBJECT DETAILS

Bacterial Strains

Bacterial strains used in this study are listed in Table S1, and are derivatives of *E.coli* strain MG1655. Cells were grown in LB. When relevant, antibiotics were added at the following concentrations: kanamycin 25μg mL^{-1}, chloramphenicol 10 μg mL^{-1}, tetracycline 10 μg mL^{-1}, ampicillin 150 μg mL^{-1} in liquid cultures or 100 μg mL^{-1} on plates. The *rne*^{ts} mutant allele was obtained from E. Massé (Massé et al., 2003).

Construction of *lacZ* fusions was by recombineering following previously described λ red-based procedures (Coornaert et al., 2013). Briefly, DNA fragments corresponding to nts −173 or −26 to +45 of *fepA* mRNA (relative to start codon), or to nts −107 to +57 of *bamA*, were amplified by PCR using Phusion high fidelity DNA polymerase. The primers used introduced sequences homologous to the $P_{Ltet0-1}$ (P_{tet}) promoter upstream of *fepA* (or *bamA*) 5′ end, and to *lacZ* from nts +28 to at least +48, in frame with the coding sequence. When needed, primers introducing mutations were used instead, or in prior PCR reactions (see Table S2). The final PCR products were recombined in the MG1508 strain, by replacing the *cat-sacB* cassette of a chromosomal P_{tet}-*cat-sacB-lacZ* construct. Recombinants were selected on LB plates without NaCl, supplemented with 6% sucrose to counterselect cells carrying *sacB*. Chloramphenicol-sensitive colonies were subsequently purified, and the final strains were checked by PCR and sequencing for the presence of the desired fusions.

METHOD DETAILS

Oligonucleotides and Plasmids

The oligonucleotides used in this study are listed in Table S2. The plasmids are all derivatives of the pBRpLac plasmid (Guillier and Gottesman, 2006). For construction of pOmrY and pOmrYmut, DNA fragments were PCR-amplified from pBRplacRybB plasmid

(Mandin and Gottesman, 2010) using pBRrev2 and either AatIIOmrY or AatIIOmrYmut primers. After DpnI digestion of the template plasmids, the DNA fragments were subsequently cleaved with EcoRI and AatII and cloned into the corresponding sites on pBRplac. The recombinant plasmids were then transformed into DH5α cells, and sequenced.

pOmrAmut and pOmrBmut plasmids were constructed using the QuikChange II site-directed mutagenesis kit (Stratagene). pOmrA and pOmrB were used as templates in PCR with oligonucleotides introducing the desired mutation (see Table S2).

β-galactosidase Assays

Overnight cultures were diluted 500-fold in fresh LB (or LB-Amp-IPTG 100 μM for strains with plasmids) and grown at 37°C to mid-exponential phase. The β-galactosidase activity was then measured as previously described (Miller, 1992). Briefly, aliquots of 200μL (for *fepA* fusions) or 500μL (for *bamA* fusions) were mixed with 800μL or 500μL, respectively, of Z buffer and lysed with toluene. After toluene evaporation at 37°C for at least 1h, specific β-galactosidase activity was assayed with 200μL ONPG at 4mg/mL and reaction was stopped with 500μL Na_2CO_3 1M. The culture final OD at 600nm (cOD600), the culture volume in each sample (v), the reaction time (rt), and the reaction final OD at 420nm (rOD420) and 550nm (rOD550) were taken into account to calculate the specific β-galactosidase activity, following this formula: $1000 * (rOD420 - (1.75 * rOD550)/cOD600 * rt * v)$. The results shown are the mean of at least three independent replicates, and error bars represent 95% confidence intervals.

RNA Extraction and Northern Blot Assays

Total RNA was extracted by the hot-phenol method (Guillier and Gottesman, 2006) either from the same cultures than those used for the β-galactosidase experiments or from cultures subjected to pulse-induction of FepA synthesis. In this latter case, overnight cultures were diluted 500-fold in fresh LB-Amp (Figure 1D) or LB-Amp-IPTG 100 μM (Figure 2) and grown at 37°C to mid-exponential phase, then shifted or not to 44°C for 15 min in presence of 250 μM dip (and IPTG for Figure 1D); RNA was extracted after this treatment. RNA was then ethanol precipitated and equal amounts of total RNA were separated on denaturing acrylamide (for sRNAs; 3.5 μg RNA loaded) or agarose (for mRNAs; 5.5 μg RNA loaded) gels, transferred to Hybond-N+ membranes and specific RNAs were detected using specific biotinylated probes and the Ambion Brightstar detection kit.

Protein Extraction and Western Blot Assays

Protein samples were prepared from the same cultures as those used for RNA extraction. Samples preparation and western blotting were as described previously (Coornaert et al., 2013), except that detection was performed with the West-Femto kit (Thermo-Scientific). The anti-FepA and the anti-S1, kind gifts from Kathleen Postle (Higgs et al., 2002) and Knud Nierhaus, were used at 1:5000 and 1:10000 dilutions, respectively.

In Vitro RNA Transcription

Templates for T7 RNA transcription were generated by PCR, using primers adding a T7 promoter upstream of the gene to be transcribed. Two G nts were added to *fepA* 5′ end to improve transcription efficiency; the 5′ end of the sRNAs was left unchanged. After purification, the PCR products were used to generate RNAs with the T7 Megascript kit (Ambion) following manufacturer's instructions. Transcripts were then phenol extracted, ethanol precipitated and finally purified with Nucleoseq columns (GE Healthcare).

In Vitro Reverse Transcription

For those experiments, 1pmol of wt or mutant *fepA* mRNA transcripts (−173 to +129 or −26 to +129) were denatured at 80°C for 3 min in the presence of 2pmol of the Cyanine-5 labeled fepToeCy5 probe and either water or 1, 5 or 10pmol of OmrY or OmrYmut sRNA. Samples were then immediately immersed in solid CO2/ethanol for 1 min and subsequently thawed on ice. 1x final concentration of AMV-buffer (Finnzymes) was added to the reactions along with 3mM final concentration of dNTPs, and samples were subsequently incubated at 37°C for 10 min to allow for transcript-sRNA annealing and folding. 1pmol of the As−14.−2 AsDNA or water was then added to the reactions, which were incubated for another 10 min at 37°C to allow for transcript-AsDNA annealing and folding. Finally, reverse-transcription was performed with 1 unit of AMV reverse transcriptase (Finnzymes) at 37°C for 20 min, and stopped with a formamide/EDTA mixture. cDNAs were fractionated by PAGE on a 6% denaturing gel along with sequencing reactions, and visualized with a Typhoon fluorescent scanner set up for Cy5 detection.

In Vitro Toeprinting and RNA Structure Probing Assays

These assays were performed essentially as in (Coornaert et al., 2013), with minor modifications that are detailed thereafter. Briefly, 0.5pmol of wt or mutant *fepA* (−173 to +129) or *bamA* (−107 to +100) transcripts were denatured at 80°C for 3 min in 10mM Tris-acetate pH7.4, 60mM NH_4Cl and 6mM β-mercaptoethanol, together with 2pmol of fepAToeCy5 or bamAToeCy5 DNA primer labeled with a Cyanine-5 at their 5′ end. When relevant, this step was performed in the presence of increasing concentrations of sRNAs or AsDNAs. Samples were then immediately immersed in solid CO2/ethanol for 1 min and subsequently thawed on ice. Magnesium was added at 10mM final concentration, and samples were incubated at 37°C for 10 min to allow for transcript-sRNA annealing and folding. Samples were then incubated at 37°C for 10 min in 0.015% triton, 3.6mM Tris-HCl pH7.5, 0.07mM EDTA pH8.0, 7% glycerol and 7mM NH_4Cl, or the same buffer supplemented with purified Hfq protein (a kind gift from Eliane Hajnsdorf). 5pmol of 30S ribosomal subunits were then added together with 1,5mM dNTPs and 15pmol $tRNA^{fmet}$, and the samples were incubated at 37°C for

10 min. Finally, reverse-transcription was performed by incubating the samples at 37°C for 20 min with 1 unit of AMV reverse transcriptase (Finnzymes) and stopped with a formamide/EDTA mixture. cDNAs were fractionated by PAGE on 6% denaturing gels along with sequencing reactions, and visualized with a Typhoon fluorescent scanner set up for Cy5 detection.

In Vitro RNA Structure Probing

RNA structure probing assays were adapted from (Coornaert et al., 2013) as follows. Samples containing 3pmol of *fepA* (−26 to +129) transcript in water were heated at 80°C for 3 min, immediately immersed in solid CO2/ethanol for 1 min and thawed on ice. They were then incubated at 25°C for 10 min in a buffer containing 10mM magnesium acetate, 50mM ammonium chloride and either 50mM sodium cacodylate pH 7.5 for DMS treatment, or 50mM sodium borate pH 8.0 for CMCT treatment. 1μg of *L.lactis* 23S rRNA was added to the samples, along with 0.1 volume of either DMS (1:20 dilution in ethanol) or CMCT (100mg/mL in CMCT buffer). Probing reactions were carried out at 25°C for 5 min for DMS modification or 10 min for CMCT modification. RNAs were recovered by ethanol precipitation, resuspended in water and denatured along with 5pmol of the fepAToeCy5 primer mentioned above at 80°C for 3 min. The samples were then immediately immersed in solid CO2/ethanol for 1 min and thawed on ice. They were subsequently supplemented with 2.5mM dNTPs, 3mM DTT, 1X superscript III buffer, and 5.6 units of Superscript III reverse-transcriptase (Invitrogen). Reverse-transcription was performed at 50°C for 30min followed by incubation of the samples at 75°C for 15 min to inactivate the enzyme. After addition of a formamide /EDTA mixture, the cDNAs were analyzed as described above for the toeprinting assays.

QUANTIFICATION AND STATISTICAL ANALYSIS

Statistical analysis for β-galactosidase assays was performed as follows: for each fusion and condition, the mean of at least three independent replicates was considered as the final β-galactosidase specific activity. The 95% confidence intervals were then calculated from the standard deviation between replicates (σ), and the number of replicates (n) as follows: $(x - 1.96 * \sigma/\sqrt{n}, x + 1.96 * \sigma/\sqrt{n})$ where x is the mean value of the considered replicates.

Quantification of the cDNA bands produced in the toeprinting assay (Figure 4C) was carried out using the ImageJ software. For each sample, the total lane signal is the sum of the bands which correspond to the full length extension signal, the toeprint signal and the antisense-mRNA duplex signal. Each signal was then expressed as the ratio over the total lane signal.